EGG-M-92501
CONF-9210204--5

PWR Depressurization Analyses[a]

D. A. Brownson
C. A. Dobbe
D. L. Knudson

EGG-M--92501

DE93 005203

Idaho National Engineering Laboratory
Idaho Falls, ID 83415

ABSTRACT

Early containment failure resulting from direct containment heating (DCH) has been identified as a potential contributor to the risk of operating a pressurized water reactor (PWR). One important factor needed to evaluate the contribution of DCH to risk is the conditional probability that, given a core melt, the primary system will be at high pressure when the reactor vessel lower head fails. Two mechanisms that could reduce the pressure during a station blackout core melt accident are discussed. First, natural circulation in the reactor coolant system (RCS) could cause a temperature-induced failure of the RCS pressure boundary, which could result in unintentional (without operator action) depressurization. Second, plant operators could open relief valves in an attempt to intentionally depressurize the RCS prior to lower head failure. Results from analytical studies of these two depressurization mechanisms for select PWRs are presented.

INTRODUCTION

Depressurization of the reactor coolant system (RCS) prior to vessel breach has been proposed as a strategy to avoid high pressure melt ejection (HPME) during severe accidents in pressurized water reactors (PWRs). The strategy was proposed as a method to reduce the public risk associated with commercial operation of PWRs. Risk reduction is expected, since the potential for direct containment heating (DCH) and the associated challenge to containment integrity should be minimized if HPME can be avoided. Analyses are being performed at the Idaho National Engineering Laboratory (INEL) to evaluate the effects of RCS depressurization in commercial PWRs. The calculations, which extend from accident initiation to lower head failure, include evaluation of both intentional[1] and unintentional[2] depressurization during a TMLB' (station blackout) transient.

Reactor operators could be directed to take actions to depressurize the RCS if specific severe accident conditions occurred. However, intentional depressurization requires more than the overt actions of the reactor operators. Specifically, equipment availability and design features of a given PWR could influence the effectiveness of the operator actions. Previous calculations[3] indicated that a late depressurization strategy could be a viable option to avoid HPM in a Surry-type PWR. Additional calculations were needed to deter-

---

a. Work supported by the U. S. Nuclear Regulatory Commission, Office of Nuclear Regulatory Research under DOE Contract No. DE-AC07-76ID01570.

mine the effectiveness of the intentional depressurization strategy in other operating PWRs.

Calculations were required to evaluate PWR response if reactor operators do not take actions to depressurize. Without operator actions, natural circulation flow patterns could develop in the vessel and in the primary coolant loops. Full loop, in-vessel, and hot leg countercurrent natural circulation modes are possible. Under such conditions, ex-vessel RCS pressure boundaries could be heated to the point of failure prior to failure of the reactor vessel lower head. Under those conditions, unintentional RCS depressurization through the ex-vessel breach, independent of operator response and other plant-specific characteristics, could be sufficient to avoid HPME.

The objective of the assessments presented in this paper is to quantify the conditions that could occur following a severe reactor accident with and without operator response. Specifically, (a) the timing and location of the initial RCS pressure boundary failure and (b) the associated RCS and containment conditions at the time of pressure boundary failure are of interest. This information can then be used to assess the potential for HPME.

In these assessments, a TMLB′ scenario (initiated by a loss of all ac power and a simultaneous loss of auxiliary feedwater) was selected as the subject core melt accident. For the intentional depressurization analyses, the RCS power-operated relief valve (PORV) was assumed to be latched open when the core exit thermocouple indicated superheated steam (922 K). The capability to simulate natural circulation in the RCS hot leg piping was incorporated into the calculations where no operator actions were assumed to appropriately represent the anticipated natural circulation flow patterns. The capability to simulate in-vessel natural circulation flow patterns was incorporated into all of the analyses. These models were based on previously reported work that investigated natural circulation cooling patterns in a Surry-type PWR under TMLB′ accident conditions.[4] The calculations were performed using the SCDAP/RELAP5/MOD3[5] computer code to calculate the plant response associated with this accident and its progression.

The unintentional depressurization calculations (no operator actions) included assessment of the HPME potential for six different cases. In the Base Case, full loop, in-vessel, and hot leg countercurrent natural circulation flows were considered. This approach is consistent with flow conditions that could be expected following TMLB′ initiation without operator interaction. Although hot leg countercurrent natural circulation is expected, uncertainties exist with respect to the effectiveness of heat transfer to ex-vessel structures. Based on these uncertainties, hot leg countercurrent natural circulation was eliminated in Case 2. As a result, Case 2 represents a bounding calculation where ex-vessel heat transfer is minimized and should reduce the time to reactor vessel failure. Cases 3 through 6 were designed to account for full loop, in-vessel, and hot leg countercurrent natural circulation, along with the effects of potential reactor coolant pump (RCP) seal leakages. Each case assumed an initial 21-gpm leakage per RCP (based on calculations for intact RCP seals subjected to normal RCS temperature and pressure[6]) up to the point where the RCP coolant saturated. The leakage rates were then increased to either 250 gpm (Case 3, highest probability leak rate) or 480 gpm (Case 4, catastrophic failure of all three RCP seal stages) per pump, based on expert opinion of RCP seal performance under severe accident conditions.[7]

Case 5 was identical to Case 3 except for the way heat transfer from molten materials was treated during relocation. In Case 3, it was assumed that molten materials would remain intact during relocation from the core to the reactor vessel lower head. This approach minimizes heat loss from the debris so that a relatively rapid thermal attack on the vessel follows. In contrast, it was assumed in Case 5 that molten materials would break up during relocation. This break-up could occur as a result of the pour interacting with vessel structures and with water below the core. However, the break-up of molten materials maximizes debris/coolant heat transfer, which delays the thermal attack on the reactor vessel until the debris has time to reheat.

Case 6 was identical to Case 4 except for the way cladding deformation was treated during core heatup. In Case 4, it was assumed that deformation was limited to 2% as a result of an oxide buildup on the outer surface of the cladding prior to the onset of ballooning. The oxide layer is relatively strong but less ductile than the underlying zircaloy. As a result, oxidized cladding tends to fracture at small deformations, leading to earlier oxidation of the inner cladding surfaces with the potential for earlier core heatup associated with the exothermic reaction. In contrast, cladding rupture was assumed at deformations of 15% in Case 6. That deformation provides a potential for larger in-core flow blockage, which could affect core heatup by reducing convective heat transfer to the steam flow (driven by natural circulation). In addition, core heat-up could increase, since the surface area available for oxidation increases with deformation.

The TMLB′ sequence analyses with intentional depressurization were performed for four representative PWR geometries. The operating PWRs in the United States were separated into the four groups based on plant parameters deemed important to the capability of a PWR to successfully implement intentional depressurization. The four groups included one group for Combustion Engineering (CE) PWRs, one group for Babcock & Wilcox (B&W) PWRs, and two groups for Westinghouse (W) PWRs.[8] The calculations were performed using the late depressurization accident management strategy described in Reference 3. The Surry calculation performed in that reference was repeated for this study using the most current version of the SCDAP/RELAP5/MOD3 computer code. This version of the computer code incorporates improvements in the thermal-hydraulics and core melt progression models, as well as error corrections to code models used in the original calculation.

The first TMLB′ analysis with intentional depressurization was performed for the Surry W 3-loop PWR, representative of the first group of W PWRs, repeating the calculation reported in Reference 3. The second analysis evaluated the capability of the Sequoyah W 4-loop PWR to successfully implement intentional depressurization. Sequoyah represents the worst-case PWR relative to the ability to successfully employ the intentional depressurization strategy in the second W group. Since no SCDAP/RELAP5 computer code model of Sequoyah currently exists, the analysis was performed by modifying the Surry PWR model parameters important to intentional depressurization to simulate the Sequoyah PWR. These parameters included initial core power level, initial steam generator liquid inventory, PORV relief capacity, and initial accumulator liquid volume and pressure. The changes were made using scaled values relative to Surry presented in Reference 8.

The third analysis was performed for the Calvert Cliffs PWR, a CE facility representative of all operating CE PWRs capable of implementing intentional depressurization. The last analysis was performed for the Oconee PWR, a B&W design representing the operating B&W PWRs. Sensitivity studies investigating the effect of the SCDAP/RELAP5 debris breakup model on RCS pressure and time to lower vessel head failure following core relocation were also performed for both Calvert Cliffs and Oconee. The effect of allowing debris breakup was evaluated for Surry in Cases 3 and 5 and, due to the similar analytical methodology employed, applied to the Sequoyah analysis.

This paper first provides an overview of the SCDAP/RELAP5/MOD3 computer code used for the analyses. Next, an overview of the Surry SCDAP/RELAP5 model is discussed, since the Surry model is representative of the models used for all the PWRs analyzed. The paper then provides a discussion of the no-operator-actions analyses results, preceded by an overview of the TMLB' transient using the sequence of events for the Surry PWR Base Case. The results for the intentional depressurization analyses are then presented. Finally, conclusions based on the analytical results are provided.

SCDAP/RELAP5/MOD3 COMPUTER CODE DESCRIPTION

SCDAP/RELAP5/MOD3 was produced by incorporating models from the SCDAP,[9] TRAP-MELT,[10,11] and COUPLE[12] codes into the RELAP5/MOD3[13] code. SCDAP models provide coding for simulation of the reactor core. TRAP-MELT models serve as the basis for simulation of fission product transport and deposition. COUPLE models provide coding to allow two-dimensional finite-element heat conduction-convection calculations at user-specified locations. COUPLE detailed thermal simulations are typically used to represent molten regions in the core or lower head. And finally, RELAP5/MOD3 models allow simulation of the fluid behavior throughout the system, as well as the thermal behavior of structures outside the core. Feedbacks between the various parts of the code were developed to provide an integral analysis capability. For example, changes in coolant flow area associated with ballooning of fuel cladding or relocation are taken into consideration in the hydrodynamics.

SCDAP/RELAP5/MOD3 uses a one-dimensional, two-fluid, nonequilibrium, six-equation hydrodynamic model with a simplified capability to treat multidimensional flows. This model provides continuity, momentum, and energy equations for both the liquid and vapor phases within a control volume. The energy equation contains source terms that couple the hydrodynamic model to the heat structure conduction model by a convective heat transfer formulation. The code contains special process models for critical flow, abrupt area changes, branching, crossflow junctions, pumps, accumulators, valves, core neutronics, and control systems. A flooding model can be applied at vertical junctions. A generalized creep rupture model, which accounts for the cumulative effects of pressure- and temperature-induced stresses, is also included for prediction of pressure boundary failures. The creep rupture model can be applied to any RELAP5/MOD3 heat structure or to any structure represented by a finite-element COUPLE mesh.

SCDAP components simulate core disruption by modeling heatup, geometry changes, and material relocation. Detailed modeling of cylindrical and slab heat

structures is allowed. Thus, fuel rods, control rods and blades, instrument tubes, and flow shrouds can be represented. All structures of the same type, geometry, and power in a coolant channel are grouped together; and one set of input parameters is used for each of these groupings or components. Code input identifies the number of rods or tubes in each component and their relative positions for the purpose of radiation heat transfer calculations. Models in SCDAP calculate fuel and cladding temperatures, zircaloy oxidation, hydrogen generation, cladding ballooning and rupture, fuel and cladding liquefaction, flow and freezing of the liquified materials, and release of fission products. Oxidation of the inside surface of the fuel rod is calculated for ballooned and ruptured cladding. The code does not calculate oxidation of material (zircaloy) during or following relocation. Interactions between molten core material and the fluid below the core are explicitly modeled. Debris formation and behavior in the reactor vessel lower head and resultant thermal attack on the vessel lower head structure by the relocated core material are also treated.

SCDAP/RELAP5/MOD3 INPUT MODEL DESCRIPTION

The PWR input models used for the analyses described in this paper utilized a common modeling philosophy. The following describes the Surry SCDAP/RELAP5 input model and, with the exception of component numbering and RCS coolant loop configuration, the following discussion applies to the CE and B&W input models as well.

The RELAP5 model was used to simulate the thermal-hydraulics of the reactor vessel, the piping in all three primary coolant loops, the pressurizer, all three steam generators, and selected parts of the secondary systems. Reactor vessel nodalization, as developed by Bayless,[4] is shown in Figure 1. As indicated, three parallel flow channels extend from the lower plenum through the core to the upper reactor vessel head. If the appropriate conditions exist, this arrangement will allow development of in-vessel natural circulation. Heat structures, which are shown as shaded areas, represent the structural mass of the reactor vessel walls, the core barrel and baffle, the thermal shield, the upper and lower core support plates, and structures in the upper and lower plena. External surfaces of all heat structures were assumed to be adiabatic.

Nodalizations of the primary coolant loop containing the pressurizer, as developed by Bayless,[4] is shown in Figure 2. With the exception of the pressurizer and associated surge line piping, similar nodalizations were included in the model to separately represent the other two primary coolant loops in the Surry PWR.

The nodalization shown in Figure 2 was used in conjunction with the reactor vessel nodalization from TMLB′ initiation to core heatup. In this assessment, it was assumed that the onset of core heatup coincided with a core exit vapor superheat of 2.78 K. During this portion of the transient, full loop natural circulation of subcooled and saturated liquid can develop. As the core heats the primary coolant toward saturation, however, voids begin to form and collect at the top of the steam generator U-tubes. Once that occurs, full loop natural circulation of liquid is interrupted.

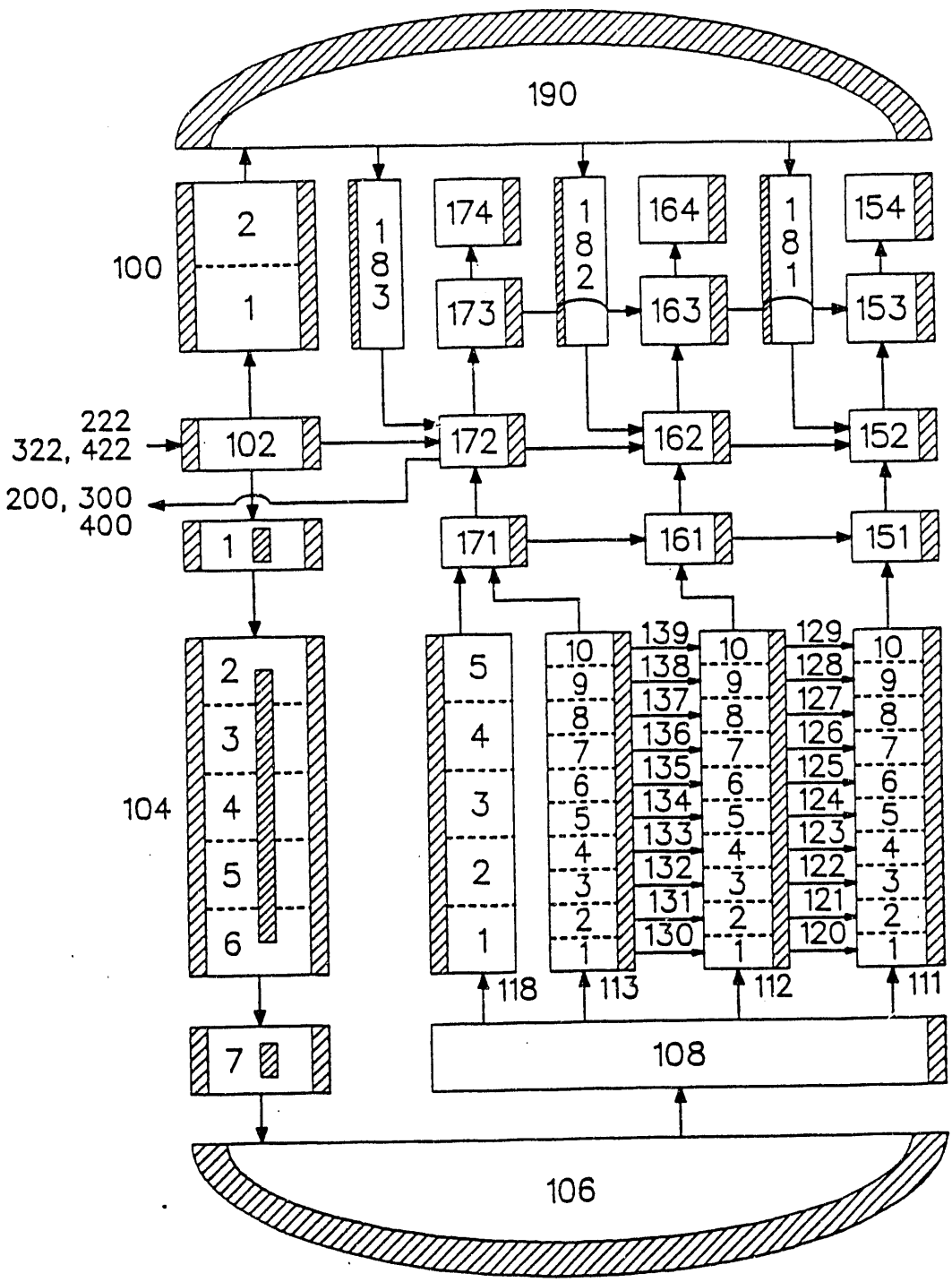

Figure 1. Surry NPP reactor vessel nodalization with provisions for in-vessel natural circulation.

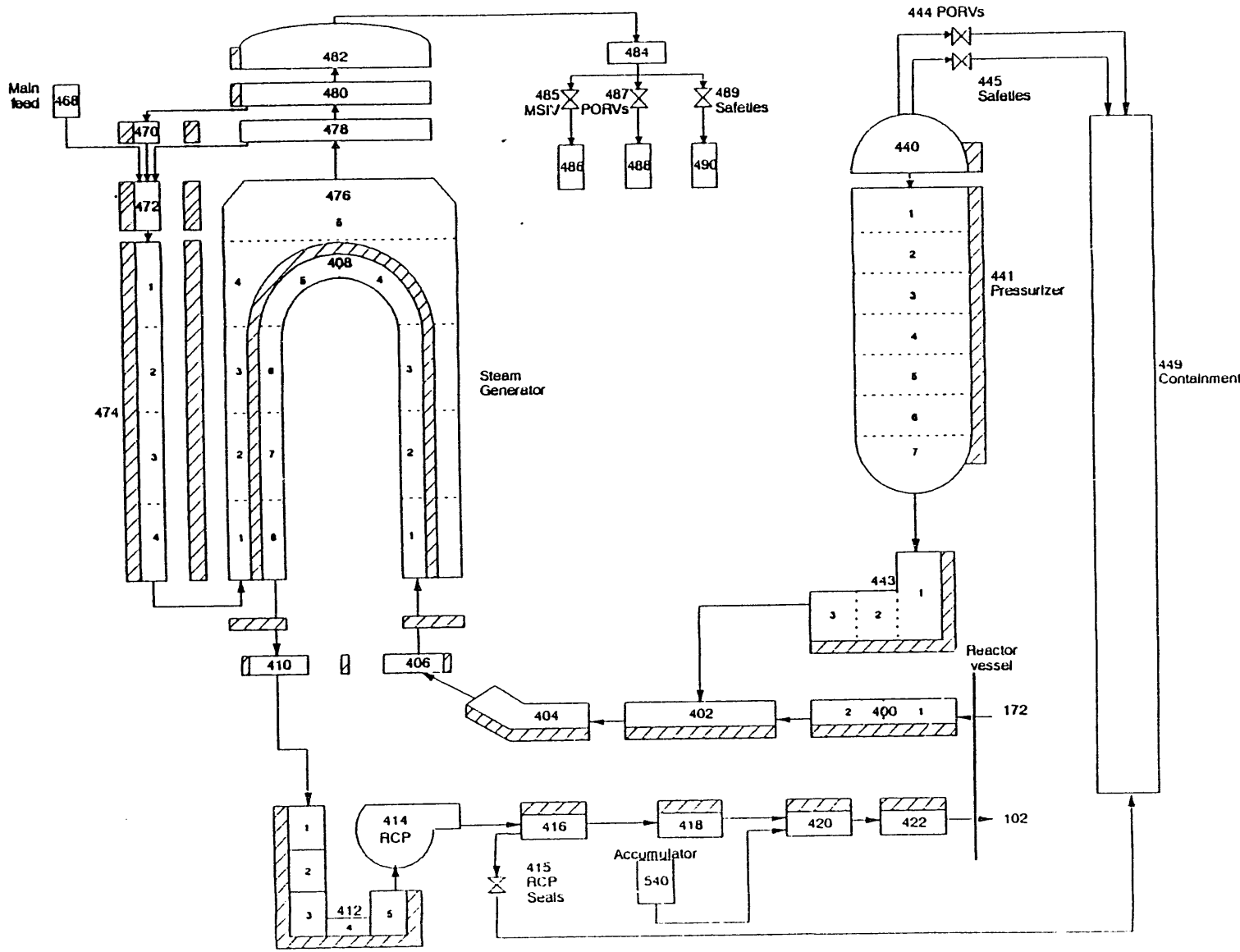

Figure 2. Pressurizer coolant loop nodalization for the Surry NPP without provisions for hot leg countercurrent natural circulation.

For the analyses assuming no operator actions, at the onset of core heatup, the Figure 2 nodalization was replaced by a more detailed representation in all calculations except those associated with Case 2. The more detailed nodalization provides the flow paths needed to represent hot leg countercurrent natural circulation. This nodalization was never used in Case 2, which was performed to evaluate conditions with minimum ex-vessel heat transfer, or in the intentional depressurization calculations, where the continued flow to the pressurizer PORV prevented hot leg countercurrent natural circulation patterns from developing. Hot leg countercurrent natural circulation becomes possible after saturated liquid in the hot legs drains to the vessel and/or flashes. At that time, temperature gradients from the core to the steam generator U-tubes can drive steam flow along the top half of the hot leg, through a portion of the steam generator U-tubes, and back to the vessel through a cooler portion of the steam generator U-tubes and the lower half of the hot leg. Note that if RCP loop seals clear, both nodalizations will allow full loop natural circulation of superheated steam. Flow areas and loss coefficients in the split hot legs, split U-tubes, and associated components were established to match experimental countercurrent flow data.[4]

The three core flow channels shown in Figure 1 were selected so that similarly powered fuel assemblies would be grouped together. A typical 15x15 fuel assembly used in Surry consists of fuel rods, control rods, and instrument tubes. In the SCDAP core models used for the subject analyses, control rods were combined with empty control rod guide tubes and instrument tubes in each core flow channel of the SCDAP/RELAP5/MOD3 model. This model simplification reduced the number of SCDAP components from nine to six by eliminating a separate component to simulate the instrument tubes and empty guide tubes in each channel.

SCDAP fuel rod components were linked to a table to provide an appropriate decay power curve for the Surry NPP following the loss of ac power (and associated reactor scram) in the analyses involving no operator actions. The decay power curve was based on an ORIGEN2 calculation used in the sensitivity calculations described by Bayless.[4] For the intentional depressurization analyses, the RELAP5 ANS79-3 kinetics model was used to allow plant-specific core parameters to be used consistently across the PWR models.

SCDAP input is required to define certain parameters that control severe core damage progression. In general, best-estimate parameters were selected where there are data or some basic understanding of the associated process. For parameters with higher degrees of uncertainty, values were selected to minimize the time to lower head failure in the analyses involving no operator actions. This approach provides the basis for a conservative evaluation of the potential for HPME, since the time available for generation of an ex-vessel failure by natural convection heating is also minimized. For the intentional depressurization analyses, the approach used was to select the best-estimate or recommended value for these parameters. Sensitivity calculations were performed for the subject analyses to ascertain the impact of the parameters on the results. A COUPLE mesh was used to represent the lower reactor vessel head in all the PWR models. The axisymetric mesh includes elements that represent the lower vessel head structure and the lower vessel head volume that receives the relocated core debris. A layer of zero-width gap elements coincided with the inner surface of the lower head. These gap elements provide a way to model contact resistance between the debris and liner. In

all the analyses, a large conductance was used to simulate perfect debris/-structure contact. This approach minimizes the time to lower head failure following relocation. The remaining elements are initially filled with primary coolant. During molten relocation, the coolant can boil-off and/or be displaced by debris.

Convection and radiation heat transfer were modeled at all interfaces between the coolant and debris. In addition, convection and radiation heat transfer were modeled along the vessel wall at all nodes that are not submerged by debris (those nodes exposed to primary coolant/steam). The external surface of the lower head was assumed to be adiabatic.

UNINTENTIONAL DEPRESSURIZATION ANALYSES AND RESULTS

The sequence of events for the Base Case calculation is given in Table 1. Following transient initiation, decay heat was transported from the core to the steam generator secondaries by natural circulation of coolant in the primary coolant loops. As the liquid in the steam generators was boiled off, the energy being removed from the RCS by the steam generators dropped below the decay heat energy being added in the core and the RCS began to heat up and pressurize. The pressurizer PORVs controlled the RCS pressurization by cycling between the opening and closing setpoints of 16.2 and 15.7 MPa, respectively. The RCS reached saturation at 6,900 s, and boiling began in the core. Voiding in the steam generator tubes terminated full loop RCS natural circulation at 7,330 s. Venting of coolant by the pressurizer PORV reduced the RCS liquid inventory until the core was uncovered at 8,750 s, initiating core heatup and superheating of steam in the RCS. The core was completely uncovered by 10,560 s, with rapid oxidation of the fuel cladding commencing at 10,770 s.

Circulation of superheated steam in the core, upper plenum, and hot legs and cyclic flow through the pressurizer PORV to control RCS pressure removed core decay heat and caused a heatup of the hot legs and pressurizer surge line structures. The heatup resulted in a calculated creep rupture failure of the pressurizer surge line piping at 14,250 s. Assuming that the pressurizer surge line did not fail, creep rupture failure of the hot leg nozzles would be calculated to occur at 15,500 s. If none of the calculated creep rupture failures occurred, ceramic melting of core material at 16,700 s would have initiated the formation of a molten pool in the core supported by a metallic crust in the bottom of the core. The lower crust was calculated to fail at 28,850 s, causing a relocation of 66,990 kg of molten core material. The lower head was predicted to fail at 28,920 s, with an RCS pressure of 16.0 MPa and a containment pressure of 0.19 MPa. The RCS pressure response was predicated on the assumption that the RCS piping failures had not occurred.

Figure 3 shows the RCS pressure response to the Base Case TMLB′ transient. The pressure initially decreased as the steam generators remove more energy than was being added by the core. The oscillations in the pressure prior to steam generator dryout at 4,700 s reflect the cycling of the steam generator secondary relief valves. Following steam generator dryout, the pressure increased to the PORV opening pressure. The pressure then cycled between the PORV opening and closing setpoint for the remainder of the transient. The

Table 1. Sequence of events for the Surry TMLB′ without intentional depressurization.

Event	Event time by Case (s)[a]					
	Base	2	3	4	5	6
Accident initiation	0	0	0	0	0	0
Start of core uncovery	8750	8750	8810	8490	8810	8490
Complete core uncovery	10560	10640	11360	10060	11360	10060
Onset of oxidation	10770	10620	11040	10770	11040	10760
Surge line failure	14250	12930	20230	---	20230	---
First fuel clad failure	14500	12360	13230	11840	13230	12000
First hot leg failure	15500	14060	20090	---	20090	---
Beginning of accumulator injections	---	---	14280	12140	14280	12160
Initial formation of in-core molten pool	16700	15180	14510	14090	14510	20700
Accumulators empty	---	---	---	21970	28500	21790
Crust failure and core relocation	28850	15470	24200	25560	24200	23030
Lower head failure	28920	15610	24340	25980	28780	23390

a. Events marked '---' were not predicted during the calculation.

sustained pressure increase starting at 7,500 s was caused by the pressurizer becoming liquid-filled and the PORV venting liquid with a lower specific energy than steam. As noted earlier, an RCS boundary breech was not associated with the creep rupture failure of the surge line or hot legs. The effect of the breech would be a rapid reduction in RCS pressure starting at 14,250 s.

Figure 4 shows the temperature of the top of the pressurizer loop hot leg nozzle and the pressurizer surge line at the entrance to the hot leg. Due to its smaller thermal mass, the pressurizer surge line heated up faster and was predicted to fail earlier than the hot leg nozzle. Note that the hot leg nozzle failure prediction was based on the assumption that no RCS boundary failure was associated with the surge line creep rupture failure prediction.

The sequence of events for Case 2 are also given in Table 1. The Case 2 sensitivity calculation produced a more rapid progression of core damage than the Base Case. By eliminating the hot leg countercurrent flow, the only structures available to absorb core heat were in the upper plenum and along the

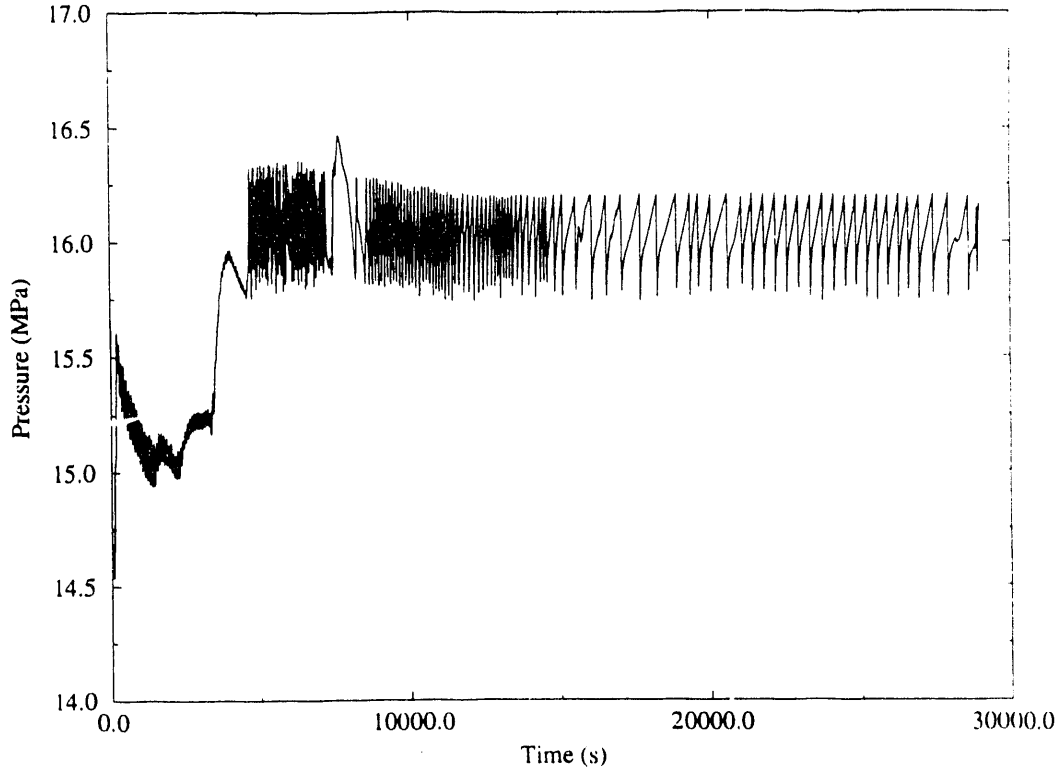

Figure 3. Reactor vessel lower head pressure vs. time for the Surry TMLB' Base Case.

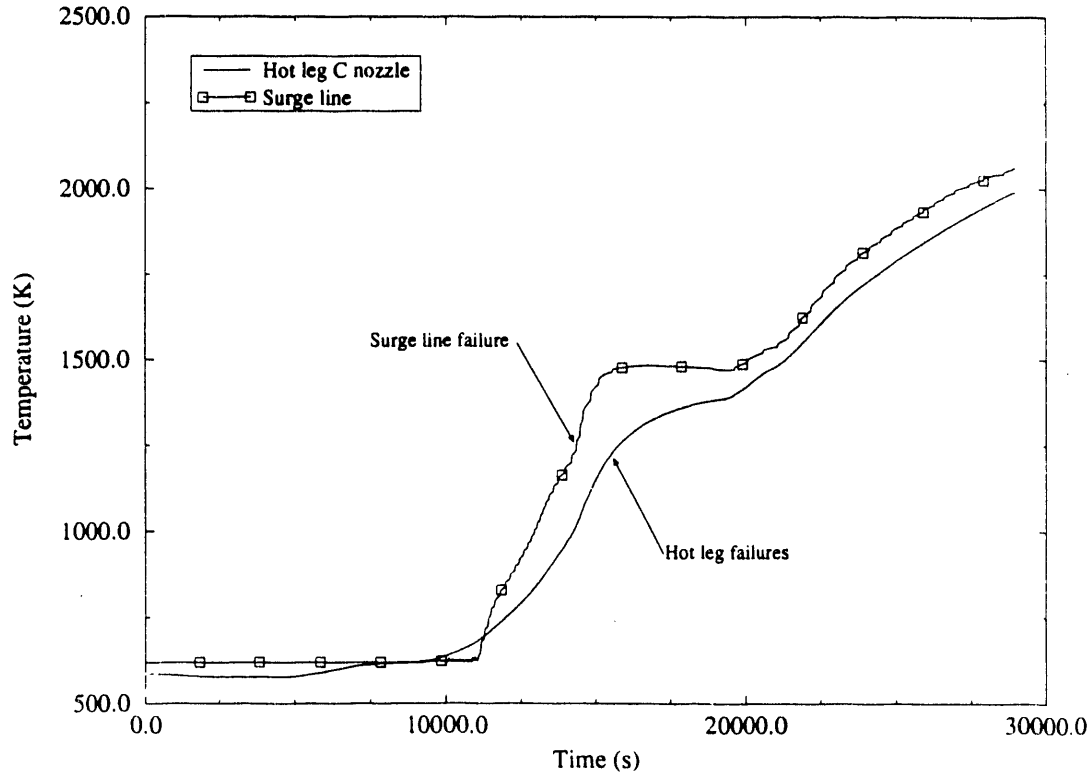

Figure 4. Hot leg and pressurizer surge line nozzle volume average structure temperature for the Surry TMLB' Base Case.

flow path from the upper plenum to the pressurizer (structure in the hot leg between the vessel and pressurizer surge line, and the pressurizer surge line). The faster core heatup produced a more rapid increase in steam temperatures than observed in the Base Case and resulted in a calculated creep rupture failure of the pressurizer surge line and the pressurizer loop hot leg nozzle 1,320 s and 1,440 s earlier than in the Base Case, respectively.

A major difference between the two calculations occurred in the core damage progression. For Case 2, the upper half of the core began meltdown at 15,180 s, 1,520 s earlier than in the Base Case. The resultant relocating Zr-UO_2 cooled and solidified at 1.10 m above the bottom of the core instead of at the core bottom, as observed in the Base Case. The initial melting of ceramic debris therefore occurred near the core midplane and had a higher heat generation rate than that formed in the Base Case. As a result, the bottom crust heated up and failed at 15,470 s; and 6,850 kg of molten core material relocated to the lower head. The massive relocation resulted in a creep rupture failure of the lower head at 15,610 s, 13,310 s earlier than in the Base Case calculation.

Case 3 was performed to evaluate the effect of RCP seal leakage on the potential for HPME through comparison to the Base Case. Before making that comparison, some details of this calculation need to be described to facilitate subsequent evaluation of the other RCP seal leak cases. The sequence of events from TMLB′ initiation to creep rupture failure of the lower head for this calculation is summarized in Table 1.

Seal leaks of 21 gpm per RCP were introduced at TMLB′ initiation to account for seal heating failure due to the loss of cooling water. Following RCP coast-down, decay heat was transported from the core and rejected to the steam generator secondaries by full loop natural circulation of subcooled and saturated liquid. At the same time, mass and energy were also removed by discharge through RCP seal leaks, leading to an RCS depressurization, as shown in Figure 5.

Following steam generator dryout, the energy removed by superheating vapor in the steam generator secondaries plus the energy discharged through the RCP seal leaks was less than the decay heat produced in the core. As a result, temperatures and pressures in the RCS began to increase. At 5,840 s, RCS pressure reached the opening setpoint of the pressurizer PORV. PORV cycling followed, which controlled RCS pressure between 15.7 and 16.2 MPa, as indicated in Figure 5.

In-core boiling and discharge through the PORV and the RCP seals reduced RCS inventory, with core uncovery beginning at 8,810 s. By 9,680 s, core energy was absorbed by heat transfer to vessel and ex-vessel structures and by discharge through the RCP seals. At that point, PORV cycling ended and a second depressurization followed, as shown in Figure 5.

Cladding oxidation in the high-temperature steam environment began at 11,040 s and gradually increased as the core uncovered. Uncovery was completed at 11,360 s. The exothermic oxidation reaction increased core temperatures, which led to fuel rod gas pressurization and the first clad rupture at 13,230 s. Clad rupture allowed double-sided oxidation, which produced an abrupt increase in core temperatures. Molten materials from the highest temperature

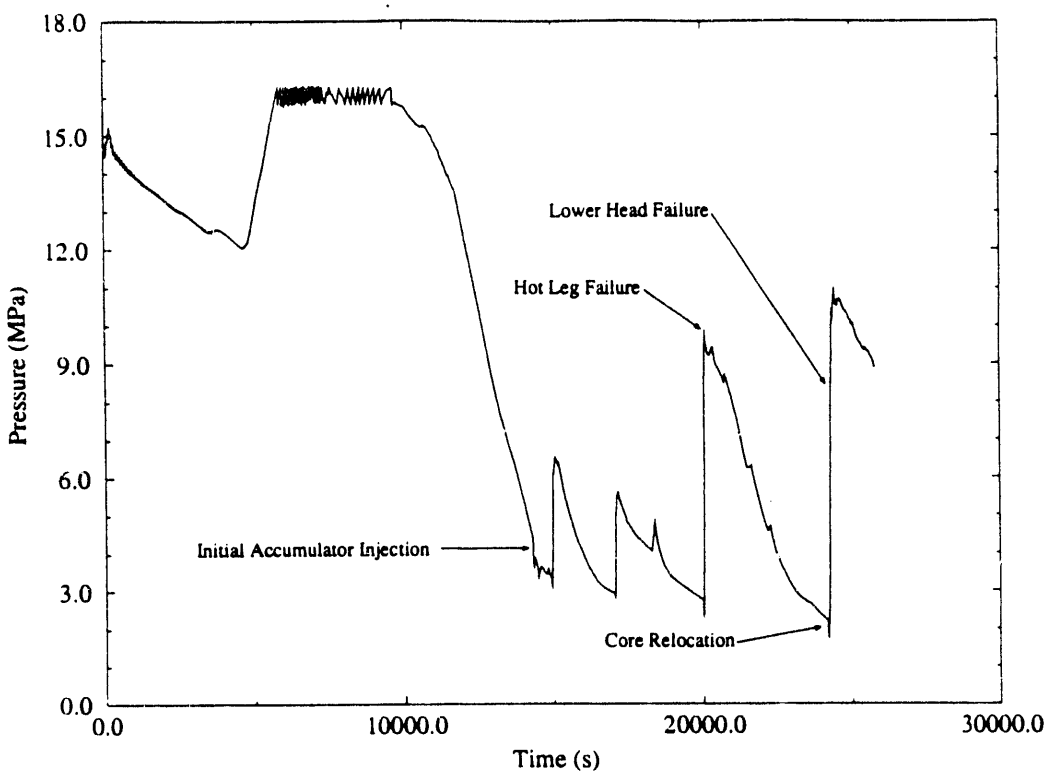

Figure 5. Reactor vessel lower head pressure vs. time for Surry TMLB' Case 3.

(highest power) regions near the center of the core began slumping shortly thereafter. A metallic crust was established as mixtures of cladding and dissolved fuel were frozen at an elevation 0.366 m above the bottom of the center channel. Meltdown in the center channel followed as a result of restricted cooling following crust formation.

RCS pressure was reduced to the initial accumulator pressure at 14,280 s by continued leakage through the RCP seals. Accumulator injection followed in four cycles. During each cycle, the RCS pressure dropped below the accumulator pressure and water was injected, cooling hot structures and core materials. Steam generated during the cooling increased RCS pressure to a point above the accumulator pressure, which terminated injection. The surge line piping was predicted to fail due to creep rupture at 20,230 s. Following the final injection cycle, a boil-off reduced crust heat transfer, leading to crust heatup and failure at 24,200 s. Crust failure allowed 12,370 kg of molten core material to relocate to the lower head. Thermal attack by the relocated core debris resulted in a creep rupture failure of the lower head at 24,340 s with an RCS pressure of 8.56 MPa and containment pressure of .16 MPa. Since creep rupture of the surge line occurred before this time, the potential for HPME should not exist under these conditions.

Case 4 was performed to evaluate the effect of depressurization rate on the potential for HPME through comparison to Case 3. This calculation was identical to Case 3 except that seal leakage was increased from 21 to 480 gpm per RCP at saturation. Thus, the sequence of events from TMLB' initiation to RCP saturation was identical to those listed for Case 3. Events from RCP saturation to creep rupture failure of the lower head are summarized in Table 1.

With respect to Case 3, the sequence of events in Case 4 is relatively early from RCP saturation to the first accumulator injection and relatively late thereafter. This relationship is consistent with the difference in RCP seal leak rates, as explained below.

Events from RCP saturation to the first accumulator injection occurred earlier in Case 4 because RCS coolant was depleted through RCP seal leaks at a faster rate. Since core uncovery began sooner and progressed at a faster rate in Case 4, the onset of core damage (oxidation, ballooning) was also relatively early. Consistent with the difference in leak rates, depressurization to the initial accumulator pressure in Case 4 was 2,140 s earlier than in Case 3.

In addition to a relatively early start on accumulator cycling, the time lag between the onset of core damage and injection was shorter in Case 4. The initial accumulator pressure was reached 1,370 s after the onset of oxidation in Case 4, while 3,280 s elapsed in Case 3. As a result, reactor vessel liquid inventory was higher in Case 4 at the onset of core degradation, somewhat delaying core relocation and lower head failure relative to Case 3.

In this calculation, a lower crust failure at 24,200 s allowed relocation of 15,120 kg of molten core material to the lower head. The resultant failure of the lower head by creep rupture was predicted at 25,980 s, some 1,550 s after lower head failure in Case 3.

All ex-vessel RCS pressure boundaries were intact at the time of lower head failure in this calculation. With an RCS pressure of 1.36 MPa at the time of vessel failure, it is clear that a potential for HPME exists in this case.

Case 5 was performed to evaluate the effect of debris/coolant interaction on the potential for HPME through comparison to Case 3. Debris/coolant interaction was varied in this calculation by assuming that molten debris would break up during relocation to the lower head. Therefore, the sequence of events from TMLB′ initiation up to the first molten relocation at lower crust failure was identical to that for Case 3. Case 5 events from accident initiation to creep rupture failure of the lower head are summarized in Table 1.

A pour of molten materials from the core is fragmented during relocation to the lower head if debris breakup is assumed (Case 5). The total heat transfer from the relocating materials is large because the surface area of the fragments exposed to the coolant is large. As a result, the pour is quenched before reaching the lower head. In contrast, molten materials pour from the core to the lower head in a coherent stream if an intact debris relocation is assumed (Case 3). Heat transfer from the molten materials is not calculated, since the exposed surface area is relatively small and the relocation period is (normally) short. The temperature of the relocated debris is initially much higher and the RCS pressure is much lower due to the lack of heat transfer to the coolant during relocation if debris breakup does not occur. The lower head was predicted to fail 4,480 s later with debris breakup (Case 5) than without (Case 3). The RCS pressure at vessel breach was 6.5 MPa. Due to earlier creep rupture failure of the RCS piping, the potential for HPME should not exist in this case (similar to Case 3).

Case 6 was performed to evaluate the effect of clad deformation on the potential for HPME through comparison to Case 4. The only difference between Cases

4 and 6 was in the specification of the maximum rupture strain, which controls the clad deformation associated with ballooning. Therefore, the sequence of events from TMLB′ initiation to the first fuel cladding failure was identical in Cases 4 and 6. Case 6 events from the first fuel cladding failure to creep rupture failure of the lower head are summarized in Table 1.

Fuel pin pressure increases with core temperature. Ballooning begins when the difference between pin pressure and RCS pressure exceeds the clad strength, and deformation terminates when the clad ruptures. In Case 6, maximum deformations of 12.5% in the center and middle and 15 % in the outer channels were predicted to occur. Those deformations were larger than the 2% rupture deformations calculated in all flow channels in Case 4.

The coolant flow area through the core is reduced in proportion to the deformation as the cladding balloons. The higher core resistance resulted in longer accumulator injection cycles due to the longer time required for accumulator water to reach the hot core surfaces and flash. The longer accumulator injections produced an earlier emptying of the accumulators than observed in Case 4.

The core heatup proceeded more rapidly in Case 6 following the last accumulator injection. As a result of the faster core heatup, the crust in Case 6 reached a temperature of 2,200 K and failed at 23,030 s, 2,530 s before crust failure in Case 4. The resulting relocation of 52,350 kg of molten core material produced an associated creep rupture failure of the lower head at 23,390 s, 2,590 s earlier than observed for Case 4.

All ex-vessel RCS pressure boundaries were intact at the time of lower head failure in Case 6. With an RCS pressure of approximately 1.4 MPa at the time of failure, it is clear that a potential for HPME exists in this case.

INTENTIONAL DEPRESSURIZATION ANALYSES AND RESULTS

This section of the paper describes the analytical results for a TMLB′ sequence incorporating an intentional depressurization accident management strategy for the Surry, Sequoyah, Calvert Cliffs, and Oconee PWRs. The Surry results are presented first, through comparison to those results obtained in the Base Case calculation. The results for the other PWR intentional depressurization analyses are compared to the Surry intentional depressurization results.

The intentional depressurization strategy would be initiated by the operator when the core exit thermocouple temperature reached 922 K. The Surry results for the Base Case should be identical up to this point. However, replacing the ORIGEN2 decay heat tables with the ANS79-3 kinetics model produced a time shift of +190 s to the beginning of core uncovery. This time shift was not significant relative to the findings for the subject analyses.

One major model change made for the Surry intentional depressurization analysis compared to the Base Case was that relocating debris was assumed to break up. Since this assumption results in the maximum heat transfer between the relocating material and the liquid in the lower head, this assumption should

result in a higher RCS pressure increase than the Base Case during relocation. In addition, since the stored energy of the relocating material is transferred to the lower head liquid, additional time would be required for the debris to heat up sufficiently to fail the lower head. This assumption should result in a longer time to lower head failure than the Base Case.

The sequence of events for the Surry intentional depressurization analysis is given in Table 2. As stated above, the sequence was identical to that observed in the Base Case up to the start of core uncovery. Due to differences in the steam generators for the PWRs analyzed, steam generator dryout time is included in the sequence of events. Steam generator dryout occurred at 4860 s. At this point, the RCS rapidly heated up and pressurized until the PORV setpoint pressure was reached at 4910 s, as shown in Figure 6. Since the RCS coolant inventory was continually being removed while the PORVs cycle, the core eventually begins to uncover at 8940 s. As the fuel cladding temperature increased, the steam became superheated. At 10,470 s, the core exit steam temperature reached 922 K and the PORVs were latched open, in accordance with the intentional depressurization strategy.

After the PORVs were latched open, the RCS pressure began to decrease until the accumulator setpoint pressure is reached. This occurs at 11,560 s, 1090 s after latching open the PORVs. This time was dependent upon three factors: (a) PORV setpoint pressure; (b) accumulator setpoint pressure; and (c) the PORV ratio.[8] The PORV setpoint pressure at Surry is typical of W nuclear power plants at 16.20 MPa. The accumulator setpoint pressure at 4.24 MPa is also typical of W plants. Finally, the PORV ratio for Surry is 1.00. Values for this ratio in other W plants range from 1.78 down to 0.75. The PORV ratio of Surry is the lowest value for W Group 1.

Once accumulator injection begins, injection cycles were predicted to continue until the accumulators empty. The RCS pressure increased following each injection due to vaporization of the accumulator liquid as it contacted hot core structures, halting the accumulator injection. The injection resumed when the RCS again depressurized via the PORVs to a point below the accumulator pressure. Between accumulator injections, the core structures began to heat up, and once the accumulator actuation pressure was reached for the next injection, this cycle was repeated. However, with each additional cycle, the core structure temperature increase was not as large and the RCS pressure increase following injection became less, as shown in Figure 6. From 16,500 s until the accumulators empty at 23,590 s, accumulator injections were smaller, maintaining a core liquid level about 1.3 m above the core inlet. The RCS pressure increase due to these smaller injections was minimal, resulting in a steady RCS pressure decrease as the accumulators emptied. Once the accumulators were completely empty, the RCS pressure smoothly decreased until core relocation began.

Because of the short time required to initially reach the accumulator setpoint pressure, only minimal core damage was predicted to occur before the first accumulator injection. Fuel rod cladding oxidation began at 10,750 s, the same time as in the Base Case, but was stopped by the accumulator injection cooling the core. Fuel cladding failure occurred at 11,220 s as a result of cladding ballooning and rupture, instead of the clad melting failure observed in the Base Case. Following accumulator injection, the center fuel channel melted and formed a molten pool starting at 27,230 s.

Table 2. Sequence of events for TMLB′ with intentional depressurization for representative PWRs.

Event	Event time (s)[a]			
	Surry	Sequoyah	Calvert Cliffs	Oconee
Accident initiation	0	0	0	0
Steam generator dryout	4860	4560	3480	900
Start of core uncovery	8940	8650	6100	1760
PORV latched open	10470	10090	9560	4570
Onset of oxidation	10750	10320	9860	4790
First fuel clad failure	11220	11080	10730	7190
Beginning of accumulator injections	11560	11530	12270	10120
Surge line failure	23580	23010	----	16940
Initial formation of in-core molten pool	27230	26700	15770	9930
Accumulators empty	23590	23772	----	----
Crust failure and core relocation	29010	30070	16990	19310
Lower head failure with/ without debris breakup	29350	30390	29060/ 17740	19660/ 19820

a. Events marked with '---' were not predicted during the calculation.

Due to the low stresses in the surge line piping, the SCDAP/RELAP5 creep rupture model did not predict surge line failure. However, using the pressure-induced stress on the surge line in conjunction with the surge line temperature profile and ultimate strength data of the surge line material, an estimate can be made of the surge line failure time. Using this criteria, it was estimated that, at the latest, the surge line would fail at 23,580 s upon reaching an average structure temperature of 1530 K.

By 28,390 s, the entire center and middle fuel channels were molten in a manner similar to that observed in the Base Case. As in the Base Case, a crust of metallic material was formed at the bottom of the core that supports the pool of molten material. Failure of the bottom crust occurred at 29,010 s with 73,741 kg of molten core material relocating to the lower head, resulting in a creep rupture failure at 29,350 s.

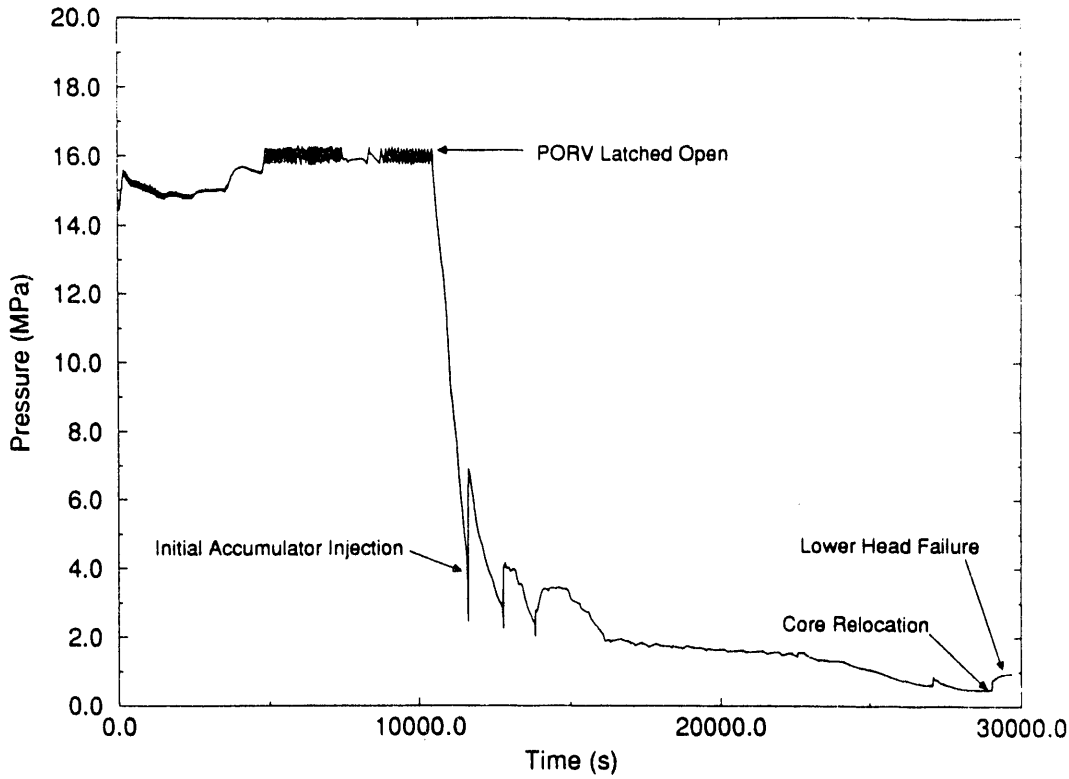

Figure 6. RCS pressure vs. time for the Surry TMLB′ with intentional depressurization.

The debris breakup assumption for this case dictates that the relocating core material will be quenched due to contact with the liquid in the lower reactor vessel. Because the energy transfer occurred rapidly during relocation, lower head liquid was either vaporized or carried out by the high steam velocities. There was insufficient liquid in the lower head 0.7 s into the core relocation to quench the relocating material and the remainder of the relocation, roughly 99% of the total mass, relocated as a cohesive molten stream, as in the Base Case. Because the amount of mass relocated with debris breakup assumed was small, the RCS pressure increase associated with quenching was also small. The RCS pressure (Figure 6) during the entire relocation rose from 0.49 MPa to only 0.78 MPa. At the time of lower head failure, RCS pressure was 0.92 MPa, with a containment pressure of 0.16 MPa. Due to the low RCS pressure at lower head failure and the anticipated surge line creep rupture failure prior to lower head failure, the potential for HPME does not exist.

The second analysis evaluated was the TMLB′ sequence with intentional depressurization for the Sequoyah PWR. As discussed earlier, the Sequoyah intentional depressurization analysis did not use a Sequoyah model; instead, the Surry model from the previous analysis was modified to simulate the Sequoyah PWR. The calculation was performed from transient initiation until lower head failure is predicted. The sequence of events is presented in Table 2.

The total secondary side water mass of the Sequoyah steam generators is smaller than Surry's (280,400 kg versus 291,000 kg); thus, as would be expected, the Sequoyah steam generators dried out earlier--in 4560 s, compared to 4860 s for Surry. Once the steam generators dried out, the RCS quickly heated up and

pressurized until the PORV setpoint pressure was reached at 4572 s. At 10,090 s, 380 s earlier than Surry, the core exit steam temperature reached 922 K and the PORVs were latched open.

Once the PORVs were latched open, the RCS pressure decreased to the accumulator setpoint pressure, as shown in Figure 7. This occurred at 11,530 s, 1440 s after latching open the PORVs. The time for RCS pressure reduction was one-third longer than was predicted for Surry. The accumulator setpoint pressure for Sequoyah is 4.65 MPa, slightly higher than the 4.24 MPa setpoint pressure of Surry. Also, the PORV ratio for Sequoyah is 0.75 compared to 1.00 for Surry. Based on these differences, it would be expected that Sequoyah would require more time to reduce the RCS pressure to the accumulator setpoint than Surry.

Once accumulator injection began, injection cycles were predicted to continue until the accumulators were empty at 23,772 s. From Figure 7, it is seen that the same pressure response during accumulator injection was observed for Sequoyah as was observed for Surry. The delay in emptying the accumulators relative to Surry is related to the smaller PORV in the Sequoyah analysis.

Because the time to reach the accumulator setpoint was longer than was predicted for Surry, more core damage was predicted to occur during this time period for Sequoyah. Fuel rod cladding oxidation was initiated at 10,320 s, and the initial fuel rod failure due to fuel rod cladding ballooning occurred at 11,080 s. Unlike the Surry calculation, the stresses in the surge line piping were sufficient to allow the SCDAP/RELAP5 creep rupture model to predict surge line failure at 23,010 s.

The center fuel channel began melting at 26,700 s. As in Surry, the molten core material was supported by a metallic crust at the bottom of the core. Failure of the bottom crust occurred at 30,070 s, with 73,828 kg of molten core material relocating to the lower head. The 1060 s delay relative to Surry was due to the protracted accumulator injection period discussed previously. The lower head was predicted to fail due to creep rupture at 30,390 s, with an RCS pressure of 0.98 MPa and a containment pressure of 0.16 MPa.

The third analysis evaluated the TMLB′ sequence with intentional depressurization for the Calvert Cliffs PWR. The calculation was performed from transient initiation until lower head failure is predicted. The sequence of events for the transient is presented in Table 2.

The total secondary side water mass of the Calvert Cliffs steam generators is equivalent to that of Sequoyah (121,474 kg for Calvert Cliffs versus 127,189 kg for Sequoyah). Although both plants have an equivalent initial thermal power (2700 MW_t for Calvert Cliffs versus 2715 MW_t for Sequoyah), Calvert Cliffs′ steam generators dried out at 3480 s, 1080 s earlier than Sequoyah's. This is a result of a much higher heat transfer rate brought about by a much higher natural circulation flow rate through the Calvert Cliffs steam generators. Once the RCS enters full loop natural circulation after the reactor coolant pumps coast down, the larger diameter of the Calvert Cliffs hot leg piping allows a mass flow rate approximately 35% higher than is calculated for Sequoyah. This allows heat to be transferred from the reactor core to the steam generators more quickly.

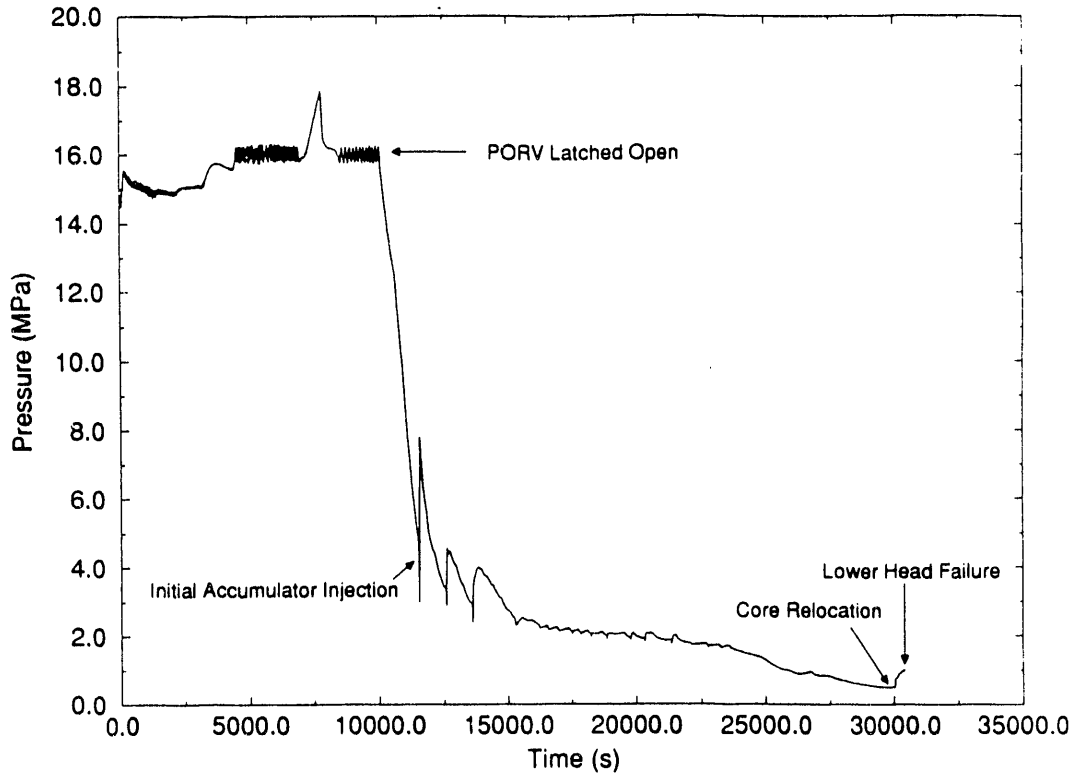

Figure 7. RCS pressure versus time for the Sequoyah TMLB' with intentional depressurization.

The PORV setpoint pressure was reached soon after steam generator dryout at 3738 s, as shown in Figure 8. The PORVs cycled to maintain RCS pressure until the core exit steam temperature reached 922 K; the PORVs were latched open at 9560 s. Once the PORVs were latched open, the RCS pressure began to decrease until the accumulator setpoint pressure was reached at 12,270 s. The RCS pressure reduction was over twice as long as predicted for Surry. The PORV setpoint pressure of 16.55 MPa for Calvert Cliffs is higher than other PWR types (16.20 MPa for W PWRs and 15.65 MPa for B&W PWRs). The accumulator setpoint pressure for CE PWRs was the lowest of any nuclear power plant type at 1.48 MPa compared to a typical value for other types of 4.24 MPa. Finally, the PORV ratio for Calvert Cliffs is 0.73 compared to Surry's value of 1.00. As a result of these factors, it would be anticipated that Calvert Cliffs would require more time to reduce the RCS pressure to the accumulator setpoint pressure.

Once accumulator injection began at 12,270 s, only three injection cycles were predicted to occur, with the last injection occurring at 20,778 s. A substantial volume of liquid was injected during each of these cycles, with 86.4% of the accumulator inventory injected prior to lower head failure. The large injections resulted from the low RCS pressure at the time of the injections. As the accumulator liquid enters the vessel, energy was removed from the vapor in the lower head to heat the injected fluid. At low pressures, the heat of vaporization is higher. As energy was removed from the vapor, it condensed; the RCS pressure decreased and more accumulator liquid was injected. This process continued until the liquid level reached the hot core structures and

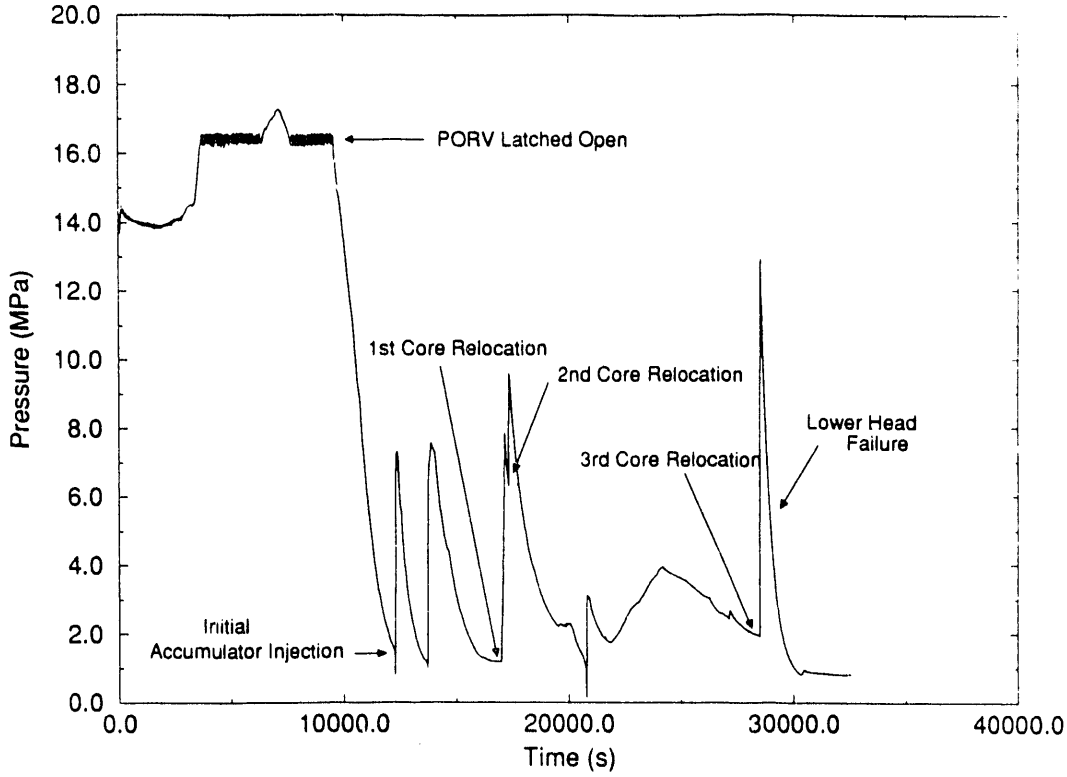

Figure 8. RCS pressure versus time for the Calvert Cliffs TMLB' with intentional depressurization.

flashed, causing the RCS pressure to increase rapidly and halting the accumulator injection.

The extended time required to reach the accumulator setpoint pressure relative to Surry resulted in more core damage before accumulator injection. Fuel rod cladding oxidation was initiated at 9860 s, and fuel rod failure due to cladding ballooning occurred at 10,730 s. The center fuel channel began melting at 15,770 s, 11,460 s earlier than Surry. This was the result of fuel rod fragmentation during the initial accumulator injection blocking flow to the center two core channels. The fragmentation resulted from the high fuel rod temperatures predicted for Calvert Cliffs. The early rod fragmentation limited the cladding oxidation to 24% of the cladding (compared to a value of 70% for Surry), since SCDAP/RELAP5 does not account for cladding oxidation after rod-like geometry is lost. The reduction in oxidation energy and core flow area reduced the core exit steam temperature and prevented the surge line piping from heating up and failing.

The molten core material was supported by a metallic crust as in the other analyses but located 1 m above the core inlet. The crust was predicted to fail at 16,990 s, with 13,087 kg of molten core material relocated. A second failure at 17,290 s relocated an additional 7,251 kg of molten core material. With the assumption that relocating debris would break up, the lower head failure time was 29,060 s, since there was sufficient liquid below the crust to quench the debris. The RCS pressure was 4.5 MPa, and the containment pressure was 0.30 MPa. With no RCS piping failures predicted, the potential for HPME exists.

A sensitivity calculation was performed to determine the effect of the debris breakup assumption. The result, as shown in Table 2, was a calculated lower head failure time of 17,740 s, 11,320 s earlier than the debris breakup case. Since the debris did not interact with the coolant in the lower head, the RCS pressure increase due to the relocation was only 1 MPa and the thermal attack on the lower head structure was much faster. The RCS pressure at lower head failure was 2.0 MPa, with an 0.24 MPa containment pressure. The potential for HPME still exists.

The final analysis evaluated the TMLB′ sequence with intentional depressurization for the Oconee PWR. The calculation was performed from transient initiation until lower head failure was predicted. The sequence of events for the transient is presented in Table 2.

The total secondary side water mass of the Oconee once-through steam generators (OTSG) is 50% of that for the Surry steam generators (70,807 kg for Oconee compared to 131,998 kg for Surry). This resulted in the steam generators drying out 900 s after transient initiation. The rapid reduction in steam generator heat transfer early in the transient results in an RCS pressure increase to the PORV setpoint 192 s into the transient, as shown in Figure 9.

Once the PORV setpoint was reached, the PORV cycled to maintain RCS pressure; but, because of the relatively small relief capacity of the Oconee PORV (13.5 kg/s compared to 45.1 kg/s for Surry), it was impossible for the PORV to maintain RCS pressure. The pressurizer filled with liquid at 1190 s, and the RCS pressure continued to increase until the pressurizer safety relief valve (SRV) setpoint was reached at 2400 s. By 3000 s, the PORV and SRVs were again discharging steam; at 3720 s, the heat removal rate through the SRVs and PORV exceeded the decay heat generation rate in the core and the RCS pressure began to decrease.

Since the RCS coolant inventory was continually being removed during this period, the core eventually began to uncover at 2430 s. The core exit steam temperature reached 922 K at 4570 s, and the PORV was latched open in accordance with the intentional depressurization strategy. This occurred soon after the SRVs ceased operation, but before the RCS pressure had dropped below the PORV closure setpoint. Once the PORV was latched open, the RCS pressure decreased to the core flood tank (CFT) setpoint pressure at 10,120 s. The time for RCS pressure reduction was over five times longer than was predicted for Surry. The PORV setpoint pressure at Oconee and other B&W plants is lower than other plant types at 15.65 MPa. The CFT setpoint pressure of Oconee is typical of the accumulator setpoint pressure of W plants at 4.24 MPa, but higher than the CE value of 1.48 MPa. Finally, the PORV ratio for Oconee is 0.24, compared to Surry's value of 1.00. From the PORV ratio alone, it would be anticipated that Oconee would require more time than was predicted for Surry to reduce the RCS pressure to the CFT setpoint pressure.

Unlike the other PWR analyses, the higher decay heat levels and extended time required to reach the accumulator setpoint pressure resulted in significant core damage for Oconee before CFT injection began at 10,120 s. Fuel rod cladding oxidation was initiated at 4790 s, and fuel rod failure due to cladding ballooning occurred at 7190 s. Over 70% of the cladding in the core was oxidized before the initial CFT injection. The fuel in the center channel began melting at 9,930 s, effectively blocking that channel from CFT cooling.

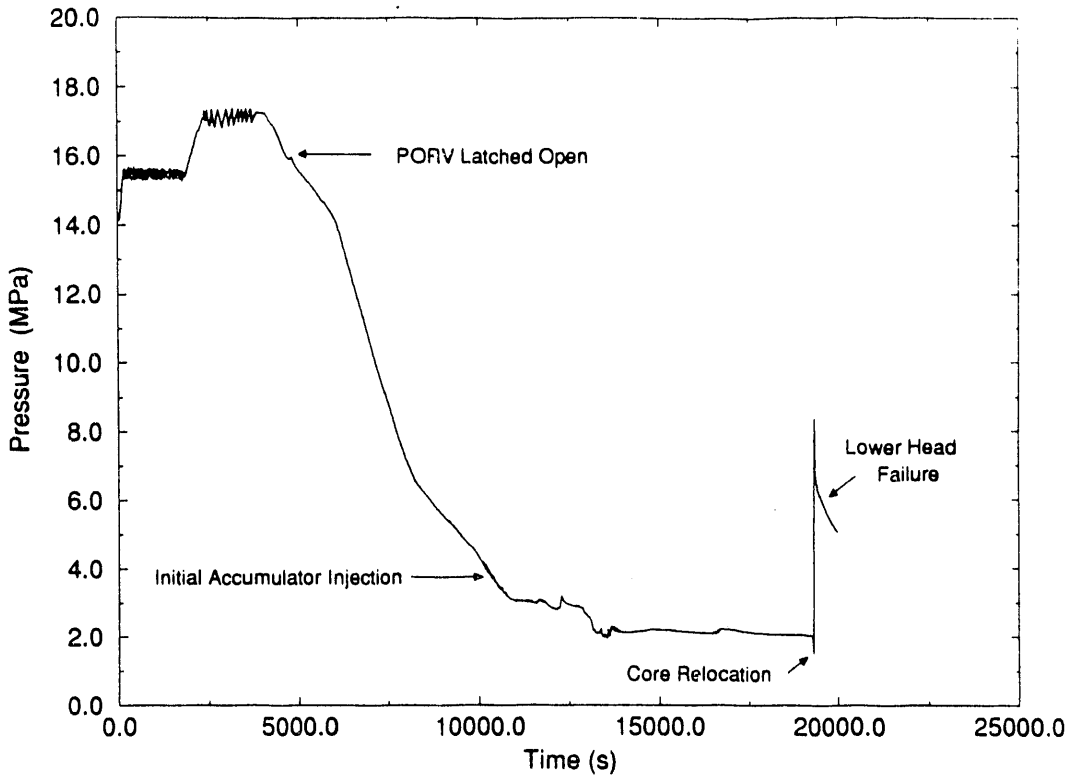

Figure 9. RCS pressure versus time for the Oconee TMLB' with intentional depressurization.

Once CFT injection began, all injection cycles have a short duration. (CFTs are equivalent to accumulators in CE and W PWRs except that CFTs inject directly into the reactor vessel instead of the cold leg piping.) This was because of the slow RCS pressure reduction caused by the small PORV capacity. The RCS pressure (Figure 9) barely decreased below the CFT setpoint before the injected liquid was vaporized, raising the RCS pressure above the CFT pressure and terminating the injection. The CFT injection period lasted 9180 s, with 54.6% of the CFT volume being injected.

Failure of the surge line was calculated to occur during the CFT injection portion of the transient. SCDAP/RELAP5 predicted creep rupture failure of the surge line at 16,800 s. An analysis of the surge line's ultimate strength was performed, using the pressure-induced stress on the surge line in conjunction with the surge line temperature profile and ultimate strength data of the surge line material (stainless steel). This analysis estimated that a surge line failure would occur at 16,940 s when the average structure temperature reached 1500 K, 138 s later than the SCDAP/RELAP5 prediction.

As the fuel channels continued to melt, a crust of metallic material was formed 0.4 m above the bottom of the core that supported the molten material. Failure of the bottom crust occurred at 19,310 s, with 99,141 kg of molten core material relocated. The relocating material was assumed to break up, and the relocating material was initially cooled by flashing coolant in the lower head to steam, shown by the rapid RCS pressure increase at this time (see Figure 9). After 24 s of relocation, there was insufficient liquid in the lower head to quench the relocating material; and the remainder of the core

material relocated over the next 192 s as a cohesive molten stream. As the molten core material relocated to the lower head in a cohesive stream, the lower head began to heat up dramatically. At 19,660 s, creep rupture failure of the lower head was predicted. The RCS pressure at the time of failure was 5.7 MPa, and the containment pressure was 0.19 MPa. If the surge line had failed as predicted, the RCS would probably have depressurized after the relocation and HPME would not be a concern.

A sensitivity analyses relative to the debris breakup assumption was performed for Oconee. If all of the relocating material was assumed to relocate as a cohesive stream, the increase in RCS pressure due to coolant flashing does not occur. The peak RCS pressure following relocation, assuming no debris breakup, was 1.7 MPa. The lower RCS pressure resulted in a predicted creep rupture failure of the lower head at 19,820 s, 160 s later than the debris breakup case. The RCS pressure at the time of failure was 1.7 MPa, and the containment pressure was 0.19 MPa. The heatup rate of the lower head was nearly the same in both calculations, since the majority of the relocation in the debris breakup calculation was in a cohesive stream.

CONCLUSIONS

The unintentional depressurization analyses for a Surry TMLB' indicate that creep rupture failures of ex-vessel piping can be expected to occur before lower head failure if the RCS is not depressurized by leaks. Under those conditions, RCS pressure will be maintained by pressurizer PORV cycling. During each valve cycle, energy will be transferred from the core to the hot leg and surge line piping. Hot leg countercurrent natural circulation will also transfer core decay heat to the loop piping. A sensitivity study showed that ignoring hot leg countercurrent natural circulation changes event timing but not the conclusion relative to HPME. The analyses show that the surge line will be the first RCS piping structure to fail. It is anticipated that the surge line failure would depressurize the RCS and effectively eliminate the potential for HPME.

A potential for HPME exists if RCS pressure is reduced below the pressurizer PORV setpoint by leaks. RCP seal leakage could produce the required reduction in RCS pressure. Surge line heating decreases significantly when the RCS pressure falls below the setpoint and PORV cycling stops. Hot leg countercurrent flow does provide a mechanism for continued heating of the hot legs. For an RCP leak rate of 250 gpm, the hot leg was predicted to fail before lower head failure, effectively eliminating the HPME concern. For a leak rate of 480 gpm, the RCS pressure reduction is sufficient to allow the heated hot legs to remain intact while core degradation progresses and molten core materials are relocated to the lower head. A subsequent thermal attack can produce creep rupture failure of the lower head long before the hot legs are heated to failure temperatures (at the reduced pressure).

For the analyses where the intentional depressurization strategy was employed to mitigate HPME concerns, the W design PWRs could successfully depressurize. For the CE PWRs, the Calvert Cliffs analysis results showed lower head failure at elevated RCS pressures as the first pressure boundary failure even with the PORV latched open. As a consequence, HPME is a concern with the intentional

depressurization strategy implemented. No assessment has been done for Calvert Cliffs for unintentional depressurization (no operator actions). For the B&W PWRs, the Oconee analysis showed that intentional depressurization would result in surge line creep rupture failure prior to lower head failure. Again, no assessment was made relative to unintentional depressurization in Oconee.

The potential for HPME was not changed in any of the analyses by variation of the core damage parameters. The changes in cladding deformation limits and debris coolant interaction did have a significant effect on the ultimate timing of lower head failure.

REFERENCES

1. D. A. Brownson et al., *Intentional Depressurization Accident Management Strategy in PWRs*, NUREG/CR-5937, EGG-2688, October 1992.

2. D. L. Knudson et al., *Assessment of the Potential for High Pressure Melt Ejection Resulting from a Surry Station Blackout Transient*, NUREG/CR-5949, EGG-2689 (Draft), November 1992

3. D. J. Hanson et al., *Depressurization as an Accident Management Strategy to Minimize the Consequences of Direct Containment Heating*, NUREG/CR-5447, EGG-2574, October 1990.

4. P. D. Bayless, *Analyses of Natural Circulation During a Surry Station Blackout Using SCDAP/RELAP5*, NUREG/CR-5214, EGG-2547, 1988.

5. C. M. Allison et al., *SCDAP/RELAP5/MOD3 Code Manual*, NUREG/CR-5273, EGG-2555 (Draft), Revision 2, Volumes 1-4, September 1991.

6. T. Boardman et al., *Leak Rate Analysis of the W Reactor Cooling Pump*, NUREG/CR-4294, 85-ETEC-DRF-1714, 1985.

7. T. A. Wheeler et al., *Analysis of Core Damage Frequency From Internal Events: Expert Judgment Elicitation*, NUREG/CR-4550, SAND86-2084, Vol. 2, 1989.

8. D. A. Brownson, *Extension of Surry Late Depressurization Strategy Results to Commercially Operating Pressurized Water Reactors*, EGG-EAST-9717, October 1991.

9. G. A. Berna, C. M. Allison, and L. J. Siefken, *SCDAP/MOD1/V0: A Computer Code for the Analysis of LWR Vessel Behavior During Severe Accident Transients*, IS-SAAM-83-002, Revision 1, July 1984.

10. H. Jordon, J. A. Gieseke, and P. Baybutt, *TRAP-MELT User's Manual*, NUREG/CR-0632, BMI-2107, February 1979.

11. H. Jordan and M. R. Kuhlman, *TRAP-MELT2 User's Manual*, NUREG/CR-4205, BMI-2124, May 1985.

12. E. C. Lemmon, *COUPLE/FLUID: A Two-Dimensional Finite Element Thermal Conduction and Advection Code*, EGG-ISD-SCD-80-1, February 1980.

13. C. M. Allison et al., *RELAP5/MOD3 Code Manual*, NUREG/CR-5535, EGG-2596 (Draft), Volumes 1-5, June 1990.

NOTICE

END

DATE
FILMED
5/13/93